

Solute transport in open channel flows and porous streambeds

Fawaz Habel^a, Cesar Mendoza^c, Amvrossios C. Bagtzoglou^{a,b,*}

^a Department of Civil Engineering and Engineering Mechanics, Columbia University, New York, NY 10027, USA

^b Department of Earth and Environmental Engineering, Columbia University, New York, NY 10027, USA

^c Department of Civil Engineering, University of Missouri, Rolla, MO 65409, USA

Received 5 March 2001; accepted 9 September 2001

Abstract

Pore-water flow inside river sediment beds resulting from water flow in the overlying river channel can strongly affect the mass and momentum transfer processes across the channel-bed interface. An analytical model for transport in porous beds, with a two-layer, coupled transport across the interface is presented. Flow and transport in the porous bed and open channel are diffusion and advection driven. The variation in the velocity profile across the flow depth, in both open channel and porous bed, is consistent with experimental studies. A slip velocity at the interface links a parabolic velocity profile in the open channel with an exponentially decaying velocity profile in the porous bed. The contaminant exchange along the interface is accounted through the imposed boundary conditions of concentration and flux continuity. The initial conditions allow the presence of solute in either or both parts of the flow domain, in order to study the transfer of solute across the interface. The Aris' method of moments is used to derive analytical expressions for the zeroth and first moments of concentration and for the velocity and effective dispersion of the solute cloud. The role of dispersion in the bed relative to dispersion in the channel was found to greatly influence the transport characteristics in the river channel-bed interface. The depth of the porous bed relative to the depth of the open channel showed a strong effect on the mean velocity of the solutes particles and the effective dispersion of the solute cloud was found to be sensitive to the flow velocity profile in the open channel in a counter-intuitive way since the transport equations are expressed in terms of axes moving with the mean particle velocity. Finally, the model was validated against experimental data from A.H. Elliott and N.H. Brooks [Water Resour. Res. 33 (1997) 123, 137]. © 2002 Published by Elsevier Science Ltd.

1. Introduction

The US Environmental Protection Agency (EPA) reported that as of 1996, about 40% of the nation's surveyed rivers, lakes, and estuaries are too polluted for basic uses such as fishing and swimming [27]. Contaminants enter our waters everyday. This contamination could originate from industrial and municipal waste discharges, runoff from urban and agricultural areas, and even individual households. Many of these pollutants have been released to the environment long ago and settled to the bottom sediments of rivers and streams, leaving hot spots of toxic substances. Once the contaminants are settled, they can act as a source or a contaminant reservoir and be released back to the water stream. Continuing uncontrolled transfer of pollutants from the contaminated bottom materials to the water

column prolongs the effects of these pollutants on organisms throughout the river ecosystem.

Therefore, transport and dispersion of solutes in open flow channels and natural rivers are of increasing interest not only as a result of its implications on water quality and major cleaning efforts but also due to the fact that the solute cannot be accurately described by a normal distribution and modeled with a Fickian-type diffusion approach. In pipes, Aris [2] described the solute distribution in terms of the moments of concentration and confirmed that it approaches the normal distribution with a variance proportional to time. However, non-normally distributed longitudinal concentration profiles are routinely found in natural rivers. The variance of the concentration distribution seems to grow more rapidly than predicted by one-dimensional models [19,20]. The traditional interpretation of these deviations is one of the following:

1. a stationary eddy structure adjacent to the porous bed where dead zones are responsible for the trapping and release of contaminant [28];

* Corresponding author.

E-mail address: abagtzog@civil.columbia.edu (A.C. Bagtzoglou).

2. a viscous sub-layer with slow moving fluid and low-intensity lateral mixing [8]; and
3. variation in flow properties across the channel, which is a general description of both (1) and (2).

The presence of stagnant dead zones along the surface of open flow has been the focus of numerous research studies [22,28]. The longitudinal spreading of contaminants along the downstream flow, the long tail of passive contaminant releases into the channel flow and the resulting skewness of the concentration's distribution are some of the effects attributed to local areas with stagnant water, for example dead zones. Valentine and Wood [28] assumed that any exchange of contaminant between the open flow and stagnant pockets is limited to diffusion and showed numerically that the time needed for the flow to reach a Gaussian-type flow can be significant in comparison to the river passage time. Fischer et al. [14], and references therein (e.g., [15]), described the variation of the concentration across the depth of the open channel and showed that the deviation of the concentration from the one predicted is largest near the channel bed. Chawin [8] explained such phenomena through the presence of a viscous sub-layer along the surface of the porous bed, in which the fluid velocity is of negligible magnitude. The channel depth was divided into two layers with linear velocity profile, uniform initial concentration, and continuous flux transformation across the interface between the two layers.

Storage of contaminant in the viscous sub-layer and its effect on transport in two-dimensional flow is not different from the retention of solute by dead zones in an open channel. A basic assumption inherent in the model of dead zones and the viscous sub-layer is the stagnant nature of the water pockets. A second assumption is the fact that interaction between the flow in the water channel and the porous structure underneath it is limited to a diffusion process driven simply by the concentration difference across the interface. However, the flow and contaminant mixing in a water channel is a much more complex process. The water present in the porous bed is far from stagnant, the flow is not uniform, and the hydrodynamic characteristics near the porous bed greatly influence mass transfer processes at the water-bed interface. Rudraiah [23] showed numerically that the velocity in the porous medium approaches the Darcy velocity at large distances from the surface, and that it is larger near the porous surface because the fluid is apt to slip at the porous surface. Nagaoka and Ohgaki [18] confirmed experimentally that the velocity profile in the porous bed of a water channel could be formulated as the sum of a Couette flow and seepage flow velocity. The Couette flow is caused by slip velocity at the porous surface decreasing exponentially with depth, and the seepage flow velocity is uniform and determined by the pressure gradient.

In summary in all the previous analytical and numerical studies, the analysis of the transient dispersion process has been limited to either the porous bed or the open channel with the mass exchange across the interface modeled as simple diffusion. The primary purpose of the present paper is to model the solute transport at the interface of an open channel and its underlying porous bed and expand the physical processes beyond the dead zones or sub-viscous layer by deriving a model whereby flow and transport in both the porous bed and the water channel are diffusion and advection-driven. The variation in the velocity profile across the flow depth is made consistent with experimental studies. A slip velocity at the interface links a parabolic velocity profile in the open channel with an exponentially decaying velocity profile in the porous bed. At the interface the velocity profile is continuous, consistent with theoretical developments by Ochoa-Tapia and Whitaker [21] who proposed a jump condition that joins naturally Darcy's law with the Brinkman correction to Stokes' equations. The contaminant exchange along the interface is accounted through the imposed boundary conditions of concentration and flux continuity. The initial conditions allow the presence of solute in either or both parts of the flow domain, in order to study the transfer of solute across the interface.

The resulting problem of two coupled partial differential equations with variable velocity coefficients is too complex for a direct analytical solution to be derived. However, the method of moments [2,3] provides an approach that allows the transformation of the problem by decreasing the number of spatial dimensions and changing the variable from concentration to the moments of concentration. Having obtained the moments of concentration, analytical expressions for the mean velocity and the effective dispersion coefficient are then derived. The dispersion coefficient provides insight into the role played by the transport in one part of the domain and the exchange across the interface on the transport pattern of the whole system. The model is also used to investigate the effect of different velocity profiles on the mean particle velocity.

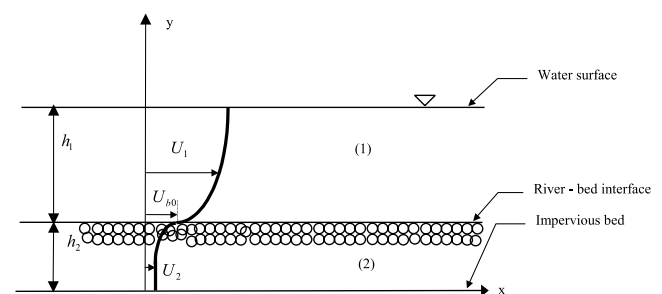


Fig. 1. A schematic description of the flow domain under consideration.

2. Mathematical model

Fig. 1 depicts the two-dimensional physical domain of the mathematical model. The water flow in the open channel is of depth h_1 , the underlying bed is of depth h_2 , and transport occurs by diffusion and advection.

The equation of the conservation of the mass is the following:

$$\frac{\partial C_i}{\partial t} + U_i(y) \frac{\partial C_i}{\partial x} = \frac{\partial}{\partial x} \left[\varepsilon_i(y) \frac{\partial C_i}{\partial x} \right] + \frac{\partial}{\partial y} \left[\varepsilon_i(y) \frac{\partial C_i}{\partial y} \right]. \quad (1)$$

The subscript ($i = 1$) denotes the free water-surface region and ($i = 2$) denotes the porous bed region. Variable C represents the average concentration across the third dimension (M/L^3), U the velocity distribution (L/T), t the time (T), x the horizontal distance (L), y the elevation above the bottom of the porous bed (L), and ε the turbulent transport coefficient (L^2/T) in the case of the open channel and the dispersion coefficient in the case of the porous bed.

The transport between regions (1) and (2) is modeled through the boundary conditions:

$$\frac{\partial C_1}{\partial y} = 0 \quad \text{at } y = h_1 + h_2 = h, \quad (2)$$

$$\frac{\partial C_2}{\partial y} = 0 \quad \text{at } y = 0, \quad (3)$$

$$C_1(x, h_2, t) = C_2(x, h_2, t), \quad (4)$$

$$\lim_{y \rightarrow h_2^+} \left[\varepsilon_1(y) \frac{\partial C_1}{\partial y} \right] = \lim_{y \rightarrow h_2^-} \left[\varepsilon_2(y) \frac{\partial C_2}{\partial y} \right]. \quad (5)$$

Boundary conditions given by (2) and (3) imply that there is no net transport across the upper and lower boundaries, whereas (4) and (5) ensure the continuity of the concentrations and fluxes at the interface. The initial conditions are for a uniformly distributed instantaneous plane source as follows:

$$C_1(x, y, 0) = \alpha \frac{m_1}{h_1} \delta(x), \quad (6a)$$

$$C_2(x, y, 0) = \beta \frac{m_2}{h_2} \delta(x), \quad (6b)$$

where α and β are constants with $\alpha = \beta = 1$ in case the solute is present in both regions, $\alpha = 1$ and $\beta = 0$ if the solute is present in region (1) only, and $\alpha = 0$ and $\beta = 1$ if present in region (2) only. m represents the number of particles released per unit width, and $\delta(x)$ is the Dirac delta function.

A constant turbulent dispersion coefficient (eddy viscosity) ε is desirable and could be assumed as

$$\varepsilon_i(y) = \varepsilon_i \quad (7)$$

if appropriate boundary conditions were to be applied, as suggested by Engelund [12,13]. In such a case, the

velocity profile in the open channel is well described by a parabolic velocity distribution obtained from integration of the flow equation, assuming a constant value of the eddy viscosity [12,13]

$$U_1(y) = U_{b0} + \frac{h_1 U_{f0}^2}{\varepsilon_1} \left[\frac{y - h_2}{h_1} - \frac{1}{2} \left(\frac{y - h_2}{h_1} \right)^2 \right] \quad (8)$$

$$\text{with } U_{b0} = K_1 U_{f0} \quad \text{and} \quad U_{f0} = \left(\frac{\tau_0}{\rho} \right)^{1/2}, \quad (9)$$

where K_1 is a constant, τ_0 denotes the bed shear stress (M/LT^2), and ρ the fluid density (M/L^3). At the porous interface, the velocity takes a finite value U_{b0} , which is known as the slip velocity. The eddy viscosity can be described as [12,13,17]

$$\varepsilon_1 = 0.077 U_{f0} h_1. \quad (10)$$

In the porous bed, the dispersion coefficient is assumed constant. Zhou and Mendoza [29] derived an exponential form for the velocity distribution that is in accordance with the work of Engelund [13], that is it ensures the continuity of the velocity distribution at the interface of the open channel and the porous bed.

$$U_2(y) = \bar{U} + (U_{b0} - \bar{U}) \exp[K_2(y - h_2)], \quad (11)$$

where \bar{U} is the uniform part of the velocity distribution and K_2 is a constant that influences the rate with which the velocity decreases with depth. For laminar flow, Zhou and Mendoza [29] showed how (11) leads to the same functional form of the boundary condition derived by Beavers and Joseph [6].

Since the solute particles will ultimately move with the mean velocity of the stream (V), it is useful to write the transport equations with respect to a coordinate system moving with velocity V . Introducing the non-dimensional variables:

$$\begin{aligned} C &= \frac{C}{c_0}, & X &= \frac{x - Vt}{h}, & T &= \frac{\varepsilon_1 t}{h^2}, & Y &= \frac{y}{h}, \\ Y_1 &= \frac{h_1}{h}, & Y_2 &= \frac{h_2}{h}, & D &= \frac{\varepsilon_2}{\varepsilon_1}, & W(\eta) &= \frac{U(y)h}{\varepsilon_1}, \\ \mathbf{Ve} &= \frac{Vh}{\varepsilon_1}, & W_{b0} &= \frac{U_{b0}h}{\varepsilon_1}, & W_{f0} &= \frac{U_{f0}h}{\varepsilon_1}, \\ \bar{W} &= \frac{\bar{U}h}{\varepsilon_1}, & \bar{K} &= hK_2, \end{aligned} \quad (12)$$

where c_0 is a reference value of C . The non-dimensional forms of Eqs. (1)–(5), (6a), (6b), (7)–(11) become

$$\frac{\partial C_1}{\partial T} + [W_1(\eta) - \mathbf{Ve}] \frac{\partial C_1}{\partial X} = \frac{\partial^2 C_1}{\partial X^2} + \frac{\partial^2 C_1}{\partial Y^2}, \quad (13)$$

$$\frac{\partial C_2}{\partial T} + [W_2(\eta) - \mathbf{Ve}] \frac{\partial C_2}{\partial X} = D \left(\frac{\partial^2 C_2}{\partial X^2} + \frac{\partial^2 C_2}{\partial Y^2} \right), \quad (14)$$

$$\frac{\partial C_i}{\partial Y} = 0 \quad Y = 1, 0, \tag{15}$$

$$C_1(X, Y_2, T) = C_2(X, Y_2, T), \tag{16}$$

$$\lim_{Y \rightarrow Y_2^+} \left(\frac{\partial C_1}{\partial Y} \right) = \lim_{Y \rightarrow Y_2^-} \left(D \frac{\partial C_2}{\partial Y} \right), \tag{17}$$

$$C_1(X, Y, 0) = \alpha \frac{m_1}{Y_1} \delta(X), \tag{18}$$

$$C_2(X, Y, 0) = \beta \frac{m_2}{Y_2} \delta(X). \tag{19}$$

The velocity profiles W_1 and W_2 are as follows:

$$W_1(Y) = W_{b0} + Y_1 W_{f0}^2 \left[\frac{Y - Y_2}{Y_1} - \frac{1}{2} \left(\frac{Y - Y_2}{Y_1} \right)^2 \right], \tag{20}$$

$$W_2(Y) = \bar{W} + (W_{b0} - \bar{W}) \exp[\bar{K}(Y - Y_2)]. \tag{21}$$

Following Aris [2], the p th spatial moment of concentration C_i is defined by

$$C_i^p = \int_{-\infty}^{+\infty} X^p C_i \, dX. \tag{22}$$

Eqs. (13)–(19) become [2,25]

$$\frac{\partial C_1^p}{\partial T} - p[W_1(Y) - \text{Ve}]C_1^{p-1} = p(p-1)C_1^{p-2} + \frac{\partial^2 C_1^p}{\partial Y^2}, \tag{23}$$

$$\frac{\partial C_2^p}{\partial T} - p[W_2(Y) - \text{Ve}]C_2^{p-1} = Dp(p-1)C_2^{p-2} + D \frac{\partial^2 C_2^p}{\partial Y^2}, \tag{24}$$

$$\frac{\partial C_i^p}{\partial Y} = 0 \quad \text{at } Y = 1, 0, \tag{25}$$

$$C_1^p(Y_2, T) = C_2^p(Y_2, T), \tag{26}$$

$$\lim_{Y \rightarrow Y_2^+} \left(\frac{\partial C_1^p}{\partial Y} \right) = \lim_{Y \rightarrow Y_2^-} \left(D \frac{\partial C_2^p}{\partial Y} \right), \tag{27}$$

$$C_1^p = \left\{ \begin{array}{ll} \alpha \frac{m_1}{Y_1}, & p = 0 \\ 0, & p \geq 1 \end{array} \right\} \quad \text{at } T = 0, \tag{28}$$

$$C_2^p = \left\{ \begin{array}{ll} \beta \frac{m_2}{Y_2}, & p = 0 \\ 0, & p \geq 1 \end{array} \right\} \quad \text{at } T = 0. \tag{29}$$

Defining μ^p as the cross-sectional average of the concentration

$$\mu^p = \int_{Y_2}^1 C_1^p \, dY + \int_0^{Y_2} C_2^p \, dY, \tag{30}$$

one can multiply Eqs. (23) and (24) by dY , and integrate using the proper boundary conditions to obtain

$$\begin{aligned} \frac{d\mu^p}{dT} = & p \int_{Y_2}^1 [W_1(Y) - \text{Ve}]C_1^{p-1} \, dY + p \int_0^{Y_2} [W_2(Y) \\ & - \text{Ve}]C_2^{p-1} \, dY + p(p-1) \int_{Y_2}^1 C_1^{p-2} \, d\eta \\ & + Dp(p-1) \int_{Y_2}^1 C_2^{p-2} \, dY. \end{aligned} \tag{31}$$

2.1. Zeroth moment of concentration

The zeroth moment of concentration (C^0) describes the mass of the solute in the system. The analytical solution for the zero moment concentrations ($p = 0$) will be derived – using the method of separation of variables – as the summation of steady state and transient solutions (Appendix A). The solution of C^0 satisfies the following equations:

$$\begin{aligned} C_1^0 = & \alpha m_1 + \beta m_2 + \sum_{n=1}^{\infty} K_n \exp(-\lambda_n^2 T) [A_1 \cos(\lambda_n Y) \\ & + B_1 \sin(\lambda_n Y)], \end{aligned} \tag{32}$$

$$C_2^0 = \alpha m_1 + \beta m_2 + \sum_{n=1}^{\infty} K_n \exp(-\lambda_n^2 T) \cos\left(\frac{\lambda_n}{\sqrt{D}} Y\right), \tag{33}$$

where λ_n are the eigenvalues of the system. The expressions for K_n , A_1 , B_1 and λ_n are derived in Appendix A.

2.2. First moment of concentration

An analysis of the variation in position of the solute cloud requires a solution for the first moment of the concentration, obtained using $p = 1$ in Eqs. (23) and (24)

$$\frac{\partial C_1^1}{\partial T} - [W_1(Y) - \text{Ve}]C_1^0 = \frac{\partial^2 C_1^1}{\partial Y^2}, \tag{34}$$

$$\frac{\partial C_2^1}{\partial T} - [W_2(Y) - \text{Ve}]C_2^0 = D \frac{\partial^2 C_2^1}{\partial Y^2}, \tag{35}$$

where C_1^0 and C_2^0 are defined by (28) and (29). The solutions of Eqs. (34) and (35) consist of a steady-state solution $g_i^1(Y)$, a complimentary solution $f_{iH}^1(Y, T)$, and a particular solution $f_{iP}^1(Y, T)$,

$$C_i^1 = f_{iH}^1(Y, T) + f_{iP}^1(Y, T) + g_i^1(Y). \tag{36}$$

The first moment is necessary for deriving the effective coefficient of the solute's cloud and the second moment of concentration. The first moment of concentration is given by

$$\begin{aligned} C_1^1 = & \sum_{n=1}^{\infty} K'_n \exp(-\alpha_n^2 T) [A'_1 \cos(\alpha_n Y) + B'_1 \sin(\alpha_n Y)] \\ & + \sum_{n=1}^{\infty} K_n F_1(Y) \exp(-\alpha_n^2 T) + g_1^1(Y), \end{aligned} \tag{37}$$

$$\begin{aligned} C_2^1 = & \sum_{n=1}^{\infty} K'_n \exp(-\alpha_n^2 T) \cos\left(\frac{\alpha_n}{\sqrt{D}} Y\right) \\ & + \sum_{n=1}^{\infty} K_n F_2(\eta) \exp(-\alpha_n^2 T) + g_2^1(Y). \end{aligned} \tag{38}$$

The functions F_i and g_i^1 , and the constants K'_n , A'_1 , B'_1 , K_n and α_n are derived in Appendix A.

2.3. Second moment of concentration

A more detailed description of the contaminant distribution needs an expression for C^2 . With $p = 2$:

$$\frac{\partial C_1^2}{\partial T} - 2[W_1(Y) - Ve]C_1^1 = 2C_1^0 + \frac{\partial^2 C_1^2}{\partial Y^2}, \tag{39}$$

$$\frac{\partial C_2^2}{\partial T} - 2[W_2(Y) - Ve]C_2^1 = D \left(2C_2^0 + \frac{\partial^2 C_2^2}{\partial Y^2} \right). \tag{40}$$

The main problem in the derivation of a complete solution for the above two equations is the fact that the expressions for C^1 are complicated. However, a solution that contains the terms that do not vanish as $T \rightarrow \infty$ can be derived, an approach previously followed by Aris [2]. Dropping the time derivative term,

$$\frac{d^2 C_1^2}{dY^2} = -2(\alpha m_1 + \beta m_2) - 2[W_1(Y) - Ve]g_1^1, \tag{41}$$

$$\frac{d^2 C_2^2}{dY^2} = -2(\alpha m_1 + \beta m_2) - \frac{2}{D}[W_2(Y) - Ve]g_2^1. \tag{42}$$

The solutions for the above two equations are obtained by simply integrating twice using the proper boundary conditions. The solutions are

$$C_1^2 = (\alpha m_1 + \beta m_2)[\Gamma_1(Y) + \Gamma_2(Y_2)], \tag{43}$$

$$C_2^2 = (\alpha m_1 + \beta m_2)[\Gamma_2(Y) + \Gamma_1(Y_2)], \tag{44}$$

where Γ_1 and Γ_2 are derived in Appendix A.

2.4. Third moment of concentration

Similar to the second moment of concentration the equations for the third moment are

$$\frac{\partial C_1^3}{\partial T} - 3[W_1(Y) - Ve]C_1^2 = 6C_1^1 + \frac{\partial^2 C_1^3}{\partial Y^2}, \tag{45}$$

$$\frac{\partial C_2^3}{\partial T} - 3[W_2(Y) - Ve]C_2^2 = D \left(6C_2^1 + \frac{\partial^2 C_2^3}{\partial Y^2} \right). \tag{46}$$

The asymptotic expressions (in time) of the above two equations are the following:

$$\frac{d^2 C_1^3}{dY^2} = -6g_1^1 - 3[W_1(Y) - Ve]C_1^2, \tag{47}$$

$$\frac{d^2 C_2^3}{dY^2} = -6g_2^1 - \frac{3}{D}[W_2(Y) - Ve]C_2^2. \tag{48}$$

The solution is achieved by double integration to obtain

$$C_1^3 = \int \int \{-6g_1^1 - 3[W_1(Y) - Ve]C_1^2\} dY dY + \int A_1 dY + A_2, \tag{49}$$

$$C_2^3 = \int \int \left\{ -6g_2^1 - \frac{3}{D}[W_2(Y) - Ve]C_2^2 \right\} dY dY + \int A'_1 dY + A'_2, \tag{50}$$

where $A_1, A_2, A'_1,$ and A'_2 are constants to be determined using the boundary conditions.

2.5. Mean particle velocity

To predict the mean particle velocity, $p = 1$ is inserted in Eq. (31) to obtain

$$\frac{d\mu^1}{dT} = \int_{\eta_2}^1 [W_1(\eta) - Ve]C_1^0 d\eta + \int_0^{\eta_2} [W_2(\eta) - Ve]C_2^0 d\eta, \tag{51}$$

where $d\mu^1/dT$ is the rate of the mean particle displacement relative to the x axis moving with the velocity Ve . The center of gravity of the cloud will ultimately move with the mean velocity of the stream (V). Thus,

$$\frac{d\mu^1}{dT} \rightarrow 0 \quad \text{as } T \rightarrow \infty$$

and

$$Ve = \frac{1}{\alpha m_1 + \beta m_2} \left[\int_{Y_2}^1 W_1(Y) \lim_{T \rightarrow \infty} C_1^0 dY + \int_0^{Y_2} W_2(Y) \lim_{T \rightarrow \infty} C_2^0 dY \right]. \tag{52}$$

Using (20) and (21) with (52) yields

$$Ve = \int_{Y_2}^1 \left\{ W_{b0} + Y_1 W_{f0}^2 \left[\frac{Y - Y_2}{Y_1} - \frac{1}{2} \left(\frac{Y - Y_2}{Y_1} \right)^2 \right] \right\} dY + \int_0^{Y_2} \{ \bar{W} + (W_{b0} - \bar{W}) \exp[\bar{K}(Y - Y_2)] \} dY. \tag{53}$$

Integration results in

$$Ve = W_{b0} Y_1 + W_{f0}^2 \left[\frac{1}{2} - Y_2 + \frac{Y_2^2}{2} + \frac{1}{2Y_1} \times \left(-\frac{1}{3} + Y_2 - Y_2^2 + \frac{Y_2^3}{3} \right) \right] + \bar{W} Y_2 + \left(\frac{W_{b0} - \bar{W}}{\bar{K}} \right) [1 - \exp(-\bar{K} Y_2)] \tag{54}$$

and

$$\frac{d\mu^1}{dT} = \sum_{n=1}^{\infty} K_n \exp(-\lambda_n T) \left\{ \int_{Y_2}^1 W_1(Y) [A_1 \cos(\lambda_n Y) + B_1 \sin(\lambda_n Y)] dY + \int_0^{Y_2} W_2(Y) \cos \left(\frac{\lambda_n}{\sqrt{D}} Y \right) dY \right\}. \tag{55}$$

It can be observed directly from (55) how $d\mu^1/dT \rightarrow 0$ at large times. Integrating once and using the condition $\mu^1 = 0$ at $T = 0$, the mean particle position is given by

$$\begin{aligned} \mu^1(T) = & \sum_{n=1}^{\infty} \frac{K_n}{\lambda_n} [1 \\ & - \exp(-\lambda_n T)] \left\{ \int_{Y_2}^1 W_1(Y) [A_1 \cos(\lambda_n Y) \right. \\ & + B_1 \sin(\lambda_n Y)] dY \\ & \left. + \int_0^{Y_2} W_2(Y) \cos\left(\frac{\lambda_n}{\sqrt{D}} Y\right) dY \right\}. \end{aligned} \tag{56}$$

Ultimately at large times, the mean particle position becomes

$$\begin{aligned} \mu^1(\infty) = & \sum_{n=1}^{\infty} \frac{K_n}{\lambda_n} \left\{ \int_{Y_2}^1 W_1(Y) [A_1 \cos(\lambda_n Y) \right. \\ & + B_1 \sin(\lambda_n Y)] dY \\ & \left. + \int_0^{Y_2} W_2(Y) \cos\left(\frac{\lambda_n}{\sqrt{D}} Y\right) dY \right\}. \end{aligned} \tag{57}$$

2.6. The effective dispersion coefficient

The effective dispersion coefficient is equal to half the temporal derivative of the variance of the contaminant cloud. In dimensionless form, the dispersion coefficient can be written as

$$De = \frac{1}{2} \frac{d\sigma^2}{dT} = \frac{1}{2} \frac{d}{dT} \left(\frac{\mu^2}{\mu^0} \right) - \mu^1 \frac{d\mu^1}{dT}. \tag{58}$$

At large times, the last component in the right-hand side of (58) approaches zero and it becomes equivalent to the equation of effective dispersion coefficient used by Aris [2] and Sumer [26]. Using Eq. (31) with $p = 2$, the dispersion coefficient becomes

$$\begin{aligned} De = & \frac{1}{2} \frac{d\mu^2}{dT} \\ = & \int_{Y_2}^1 [W_1(Y) - Ve] C_1^1 dY + \int_0^{Y_2} [W_2(Y) - Ve] C_2^1 dY \\ & + \int_{Y_2}^1 C_1^0 dY + D \int_0^{Y_2} C_2^0 dY - \mu^1 \frac{d\mu^1}{dT}. \end{aligned} \tag{59}$$

Inserting (37) and (38) into (59), one obtains

$$\begin{aligned} De = & \int_{Y_2}^1 [W_1(Y) - Ve] \left\{ \sum_{n=1}^{\infty} K'_n \exp(-\alpha^2 T) [A'_1 \cos(\alpha_n Y) \right. \\ & + B'_1 \sin(\alpha_n Y) + \sum_{n=1}^{\infty} K_n F_1 \exp(-\lambda^2 T) + g_1^1 \left. \right\} dY \\ & + \int_0^{Y_2} [W_2(Y) - Ve] \left\{ \sum_{n=1}^{\infty} K'_n \exp(-\alpha^2 T) \right. \\ & \times \cos\left(\frac{\alpha_n}{\sqrt{D}} Y\right) + \sum_{n=1}^{\infty} K_n F_2 \exp(-\lambda^2 T) + g_2^1 \left. \right\} dY \\ & + \int_{Y_2}^1 C_1^0 dY + D \int_0^{Y_2} C_2^0 dY - \mu^1 \frac{d\mu^1}{dT}. \end{aligned} \tag{60}$$

2.7. Large time approximation of the effective dispersion coefficient

At large times, the dispersion coefficient approaches the following asymptotic value:

$$\begin{aligned} De = & \int_{Y_2}^1 [W_1(Y) - Ve] g_1^1 dY + \int_0^{Y_2} [W_2(Y) \\ & - Ve] g_2^1 dY + (\alpha m_1 + \beta m_2)(Y_1 + DY_2). \end{aligned} \tag{61}$$

Integrating the above equation, arranging terms and using integral tables [1], the following analytical expression is obtained:

$$De = (\alpha m_1 + \beta m_2)(I_1 + I_2 + Y_1 + DY_2), \tag{62}$$

where

$$\begin{aligned} I_1 = & \Phi_1 p_1 Y_1 + \left(\frac{\Phi_1 p_2}{2} + \frac{\Phi_2 p_1}{2} \right) (1 - Y_2^2) \\ & + \left(\frac{\Phi_1 p_3}{3} + \frac{\Phi_2 p_2}{3} + \frac{\Phi_3 p_1}{3} \right) (1 - Y_2^3) \\ & + \left(\frac{\Phi_1 p_4}{4} + \frac{\Phi_2 p_3}{4} + \frac{\Phi_3 p_2}{4} \right) (1 - Y_2^4) \\ & + \left(\frac{\Phi_1 p_5}{5} + \frac{\Phi_2 p_4}{5} + \frac{\Phi_3 p_3}{5} \right) (1 - Y_2^5) \\ & + \left(\frac{\Phi_2 p_5}{6} + \frac{\Phi_3 p_4}{6} \right) (1 - Y_2^6) + \frac{\Phi_3 p_5}{7} (1 - Y_2^7), \end{aligned} \tag{63}$$

$$\begin{aligned} I_2 = & \exp(\bar{K} Y_2) \left[\frac{\Phi_5 q_1}{\bar{K}} + \frac{\Phi_5 q_3}{\bar{K}} Y_2^2 + \frac{\Phi_5 q_4}{2\bar{K}} + (\bar{K} Y_2 - 1) \right. \\ & \times \left(\frac{\Phi_5 q_2}{\bar{K}^2} - 2 \frac{\Phi_5 q_3}{\bar{K}^3} \right) \left. \right] + \frac{\Phi_4 q_4}{\bar{K}} - \frac{\Phi_5 q_1}{\bar{K}} + \frac{\Phi_5 q_2}{\bar{K}^2} \\ & - 2 \frac{\Phi_5 q_3}{\bar{K}^3} + \Phi_4 \left(q_1 Y_2 + q_2 \frac{Y_2^2}{2} + q_3 \frac{Y_2^3}{3} \right) \\ & + \exp(-\bar{K} Y_2) \left(-\frac{\Phi_5 q_4}{2\bar{K}} - \frac{\Phi_4 q_4}{\bar{K}} \right). \end{aligned} \tag{64}$$

The last two terms in (62) are the contributions of the initial concentration diffusion and are negligible in comparison with the first two terms, which are due to the velocity gradient in the open channel and the porous bed. Parameters $\Phi_1, \Phi_2, \Phi_3, \Phi_4, \Phi_5, p_1, p_2, p_3, p_4, p_5, q_1, q_2, q_3, q_4$, can be found in Appendix A.

3. Model testing and validation

The best method to test and validate a model is to compare it with both established analytical models and experimental data. To accomplish this, an analytical approach is used first in order to validate the analytical solutions, presented in this paper, by simplifying the model so as it matches models to which analytical solutions are already available and published. Then, making some assumptions about the flow in the water channel and the porous bed, the depth profiles of the

solutes presented in [10,11] are compared to the analytical solutions of this paper by reconstructing the analytical expression of the concentration from its known moments.

3.1. Testing with known analytical solutions

Starting with the zeroth moment of concentration, we assume that initially, the solute is uniformly distributed across the depth of the flow domain. In such a case, and for $Y_1 = Y_2 = 0.5$ the parameters $\alpha = \beta = 1$ and $m_1 = m_2 = 0.5$. Replacing these variables in (A.9) and (A.10a), (A.10b), we find that $\Delta_1 = \Delta_2 = 0$ and $K_n = 0$. As a result, $C_1^0 = C_2^0 = 1$ for all times as previously obtained by Sumer [26] and Chatwin [8]. This result states simply that the total amount of solute is constant.

In the case of the first moment of concentration, a constant and uniform diffusivity is assumed for both porous bed and open channel ($D = 1$).

As $T \rightarrow \infty$,

$$C_{1\infty}^1 = - \int_0^Y [W_1(Y) - Ve] dY$$

and

$$C_{2\infty}^1 = - \int_0^Y [W_2(Y) - Ve] dY.$$

The above two equations are equivalent to Eqs. (41) and (42) in [26].

3.2. Testing with published experimental data

In terms of experimental data, several researchers have examined porous bed–water exchanges in the field and described the exchange as a vertical advection–diffusion process with calibrated exchange parameters or as lumped-parameter or linear time series models with calibrated parameters [5,10]. Rutherford et al. [24] related the benthic oxygen uptake to bed–stream exchange mechanism and deoxygenation rates within the bed and observed that there can be rapid exchange of pore fluid into the fluidized bed material at the crest of dunes. Nagaoka and Ohgaki [18] measured the flow velocity profiles for flow over the porous bed and below the water–bed interface and related the measured diffusion coefficients in the porous bed to the intensity of turbulence. Recently, Elliott and Brooks [10,11] conducted theoretical and laboratory experiments for studying the transfer of nonsorbing solutes to a streambed with bedforms. They attempted to predict the exchange resulting from the presence of the bedforms in a steady flow for both stationary and moving bedforms.

Unfortunately, most experimental efforts that have collected data focused on a single aspect of the problem such as the velocity profile [18] or the transport and dispersion of the contaminant cloud in either the porous

bed [10,11] or the channel. No data set that captures the macroscopic processes of the transport problem as well as the interaction among those processes has been made available from all the studies discussed above and is, therefore, still to be collected. Nevertheless, making the necessary assumptions about the flow in the water channel and the porous bed, the depth profiles of the solutes presented in [10,11] are compared to the analytical solutions of this paper by reconstructing the analytical expression of the concentration from its known moments. This is accomplished using the Edgeworth form of the Gram–Charlier series [4,7,16].

This method approximates the concentration by an infinite Hermite series with the first few terms being functions of the mean and the variance. The method uses higher-order moments to expand the series beyond the Gaussian distribution, which is simply based on the first three moments (zeroth, first, and second). The series has the following form:

$$C = \frac{C_0}{\sqrt{2\pi\sigma^2}} \exp\left(-\frac{\xi^2}{2}\right) \left[1 + \frac{\chi}{6} H_3(\xi) + \dots\right], \quad (65)$$

where C_0 is the zeroth-moment concentration,

$$\sigma^2 = \left(\frac{C_2}{C_0}\right) - \left(\frac{C_1}{C_0}\right)^2,$$

$$\xi = \frac{X - (C_1/C_0)}{\sigma},$$

$$\chi = \frac{1}{\sigma^3} \left[\frac{C_3}{C_2} - 3\sigma^2 \frac{C_1}{C_0} + \left(\frac{C_1}{C_0}\right)^3 \right],$$

and

$$H_3 = \xi^3 - 3\xi.$$

One of the limitations of this method is that it fails to produce good results when the concentration distribution deviates strongly from the Gaussian shape. If the tail of the non-Gaussian distribution is of interest, an alternative approach such as the maximum entropy method could be pursued.

In Fig. 2, the analytical solution for the relative concentration, as reconstructed from the asymptotic distribution of the first four moments, is compared to the experimental data of Elliott and Brooks [11] for both a stationary natural bedform as well as for a flat bed. The experimental parameters for both runs, as reported in [11], and the appropriate model parameters are presented in Table 1. For the natural bedforms (Fig. 2(a)) and unlike the experimental solute distribution, the analytical solution does not exhibit the presence of a region with uniform concentration just below the bed surface. It does, however, approximate the experimental data quite nicely in an average sense. As pointed by Elliott and Brooks [11], this can be explained by the

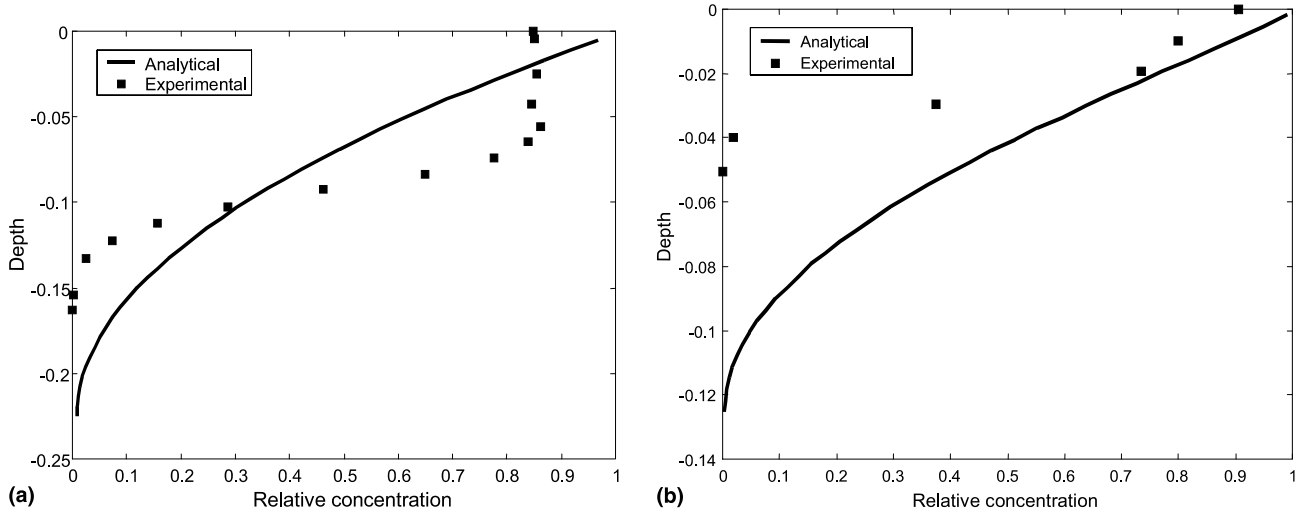


Fig. 2. Comparison of experimental data and analytical results for (a) stationary natural bedforms (Run 17 of [11]) and (b) flat bed (Run 3 of [11]).

Table 1
Measured experimental parameters from [11] and appropriate model parameters

Parameter	Description	Run 3 (flat bed)	Run 17 (natural bedforms)
U_{b0}	Slip velocity	16.8 (cm/s)	8.7 (cm/s)
\bar{U}, u_m	Constant (seepage) velocity	0.00003 (cm/s)	0.00003 (cm/s)
h_1	Height of water channel	5.15 (cm)	6.45 (cm)
h_2	Height of porous bed	12.5 (cm)	22.5 (cm)
T	Time	1 day	19 days

dominance of advection over diffusion along the depth of the experimental study.

For the test with a flat bed, the analytical solution shows a poor fit (Fig. 2(b)) despite the fact that in this case the effect of vertical advection is less pronounced. This, however, is due to the obvious disparity between the time when the data have been collected and the asymptotic nature of the analytical solution.

4. Analysis and discussion

The experiments of Nagaoka and Ohgaki [18] were used as the basis for determining the parameters used in the sensitivity analysis presented in this paper. The slip velocity was chosen from the range measured in the experiments. Four different velocity profiles were specified with constant seepage velocity and constant K_2 similar to those of the experiments of [18] and are depicted in Fig. 3 in dimensionless terms. The constant K_2 influences the rate with which the velocity decreases with depth and it ensures that the velocity approaches its asymptotic value within a narrow depth of the porous bed [29]. Table 2 lists the parameters used to describe the four velocity profiles. The analysis was limited to the case of the contaminant being initially confined to the flow in the open channel ($\beta = 0$).

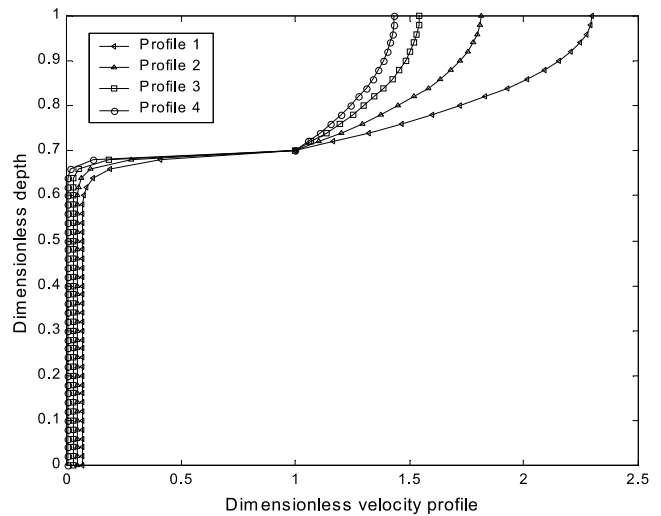


Fig. 3. Profiles of the velocity distributions scaled by the slip velocity. Note that the water channel–porous bed interface is located at a dimensionless depth of 0.7.

A MATLAB code was developed to compute the zeroth and first moments in their full transient mode, the second and third moments in their asymptotic mode, as well as other expressions of interest. Eq. (A.6) was solved for the eigenvalues in the range 0 to 4π , which proved sufficient to guarantee the convergence of the series of moments. The expression given in (62) for the

Table 2
Parameters used in the sensitivity analysis

Parameter	Description	Profile 1	Profile 2	Profile 3	Profile 4
U_{b0}	Slip velocity	15 (cm/s)	15 (cm/s)	15 (cm/s)	15 (cm/s)
U_{f0}	Friction velocity	3 (cm/s)	1.87 (cm/s)	1.25 (cm/s)	1 (cm/s)
\bar{U}	Constant velocity	1 (cm/s)	0.7 (cm/s)	0.4 (cm/s)	0.1 (cm/s)
K_2	Velocity decay factor	50	70	90	110
h_1	Height of water channel	30 (cm)	30 (cm)	30 (cm)	30 (cm)
h_2	Height of porous bed	70 (cm)	70 (cm)	70 (cm)	70 (cm)
α_1	Constant factor	1.0	1.0	1.0	1.0
m_1	Initial mass of solute in zone 1	1.0	1.0	1.0	1.0
β_1	Constant factor	0.0	0.0	0.0	0.0
m_2	Initial mass of solute in zone 2	0.0	0.0	0.0	0.0

effective diffusion was computed for different values of the relative diffusivity ($D = \varepsilon_2/\varepsilon_1$) and for different velocity profiles. The results presented in Fig. 4 show that as the relative diffusivity of the porous bed increases the dispersion coefficient decreases.

Also, for small values of the relative diffusivity of the porous bed, the effective dispersion coefficient grows very rapidly. This can be explained by noting that as D approaches zero, the flow behaves as if the porous bed were simply an impermeable boundary with the flow being only controlled by the velocity and diffusion in the open channel with a zero-flux boundary at the interface. As D increases, the flow into the porous bed comes into play and solute is exchanged across the interface, with less solute left in the open channel to contribute to the flow and dispersion. As D gets larger, the porous bed acts as a stronger sink of solute until a steady-state distribution is reached when the cloud travels with constant dispersion. For a fixed value of D , effective dispersion seems to decrease as the flow velocity increases (Fig. 4). This is counter intuitive and is due to

the fact that the transport equations are expressed in terms of a coordinate system moving with the mean particle velocity. For fixed axes, dispersion increases as the flow velocity increases. Fig. 5 shows the variation of the mean particle velocity with the friction velocity for three configurations that differ in terms of the ratio of the porous bed depth over the depth of the water in the open channel. This ratio is 1.0, 1.5, and 2.3 for Case 1, 2, and 3, respectively. The mean particle velocity is sensitive to the depth of the river porous bed relative to the depth of the open channel flow and increases as the ratio increases.

The time needed to reach steady state depends very much on D , assuming that all other variables are kept constant. For the case of $D = 1$, the zeroth moment of concentration reaches a steady-state distribution across the domain after $T = 0.5$, a value similar to the one obtained by Sumer [26] for the case of buoyant particles. However, in the case of smaller relative diffusivity ($D = 0.001$), it takes a much longer time for the solute to reach a steady-state uniform distribution (Fig. 6(a)).

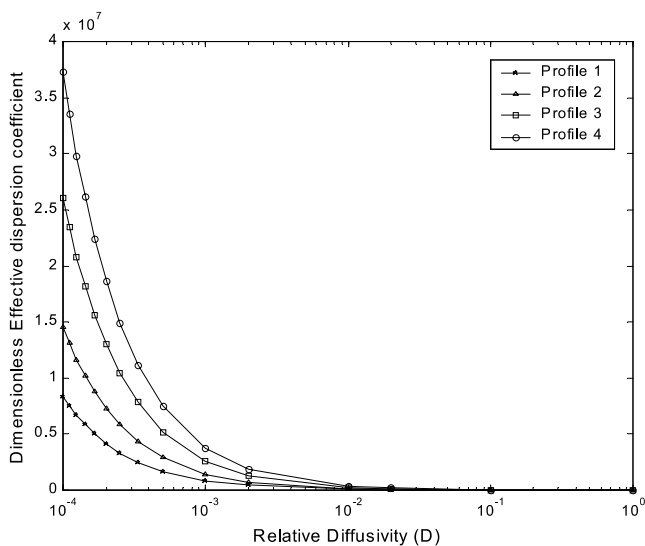


Fig. 4. Effect of relative diffusivity on the effective dispersion coefficient for different velocity profiles.

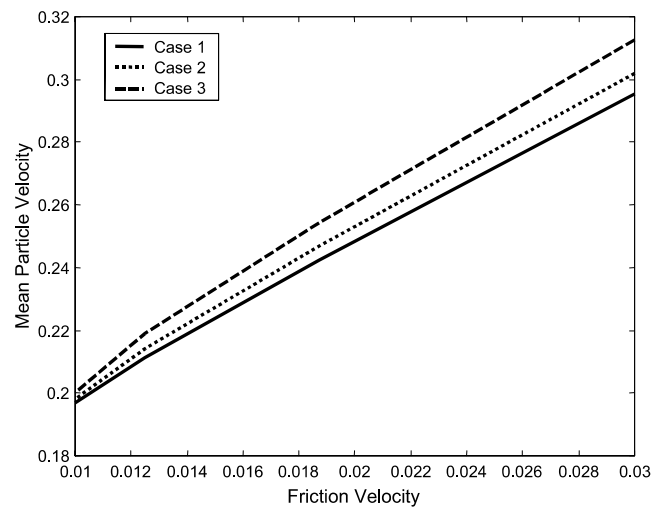


Fig. 5. Variation of the mean particle velocity with the friction velocity for three configurations with different ratios of the porous bed depth over the depth of the water. This ratio is 1.0, 1.5, and 2.3 for Case 1, 2, and 3, respectively.

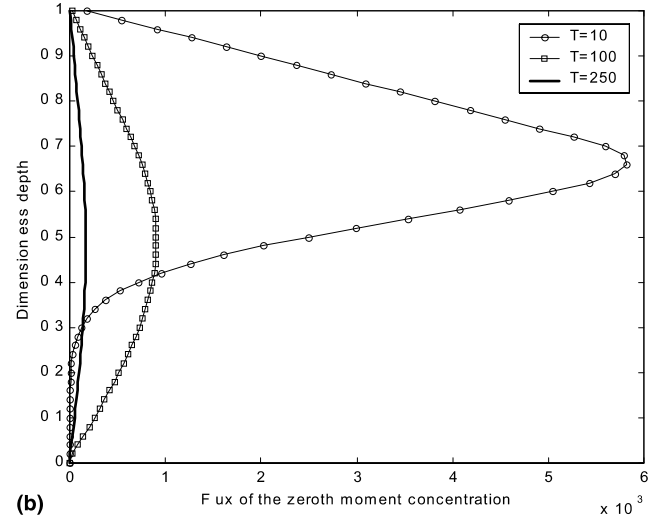
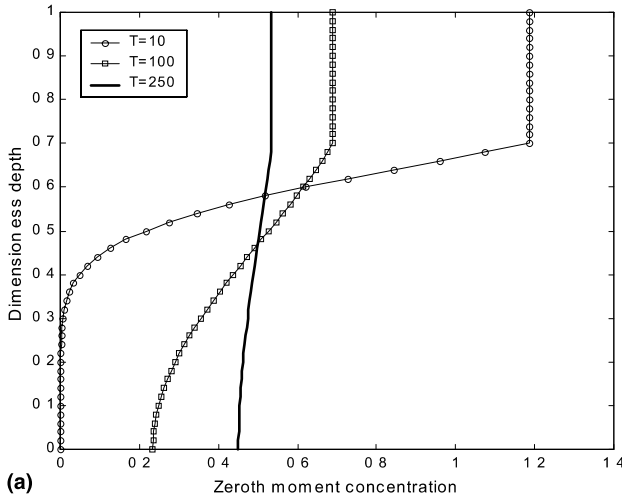


Fig. 6. Variation of (a) the zeroth moment of concentration and (b) the flux of the zeroth moment of concentration with depth for $D = 0.001$ at three different times.

It should be noted that even at $T = 250$ the flux of the zeroth moment of concentration has yet to reach the value of zero (Fig. 6(b)). This can be simply explained by the fact that a smaller diffusivity in the porous bed does not allow the solute coming from the open channel to penetrate quickly and the exchange of solute becomes a very slow process.

This is evident when comparing Figs. 6(b) and 7. In Fig. 6(b) (case with $D = 0.001$) the flux between the two parts of the domain is orders of magnitude smaller than the case with $D = 1$ (Fig. 7). This result may have important implications on efforts directed toward river cleaning. In the case of contaminant confined to the porous bed – as would be the case after a contaminant cloud moves past a specific stretch of the river – the

process by which the contaminant would leave the porous bed and enter the open channel is very slow. This process can be orders of magnitude longer than the time allocated for the cleaning of the river. This explains many site observations where concentration would increase again after the halting of the cleaning effort.

5. Summary and conclusions

In this work, we presented an analytical model for the coupled transport of solutes in open channel flow and the underlying porous bed. The transport in each domain is described by a two-dimensional advection–diffusion equation with the exchange between the two domains modeled through boundary conditions that ensure the continuity of concentration and flux at the interface. The model assumes a velocity profile that is consistent with experimental studies in both the open channel and the porous bed [18]. The slip velocity at the interface links the parabolic velocity profile in the open channel with the exponentially decaying velocity profile in the porous bed.

Using the method of moments, the model provides analytical solutions for the moments of concentration in both the water flow as well as the porous bed. An analysis of the mean particle velocity showed the effect of the depth of the porous bed relative to the depth of the open channel on the mean velocity of the solutes particles. It also showed that the effective dispersion of the solute cloud is sensitive to the flow velocity profile in the open channel in a counter-intuitive way since the transport equations are expressed in terms of axes moving with the mean particle velocity. The role of dispersion in the bed relative to dispersion in the channel was

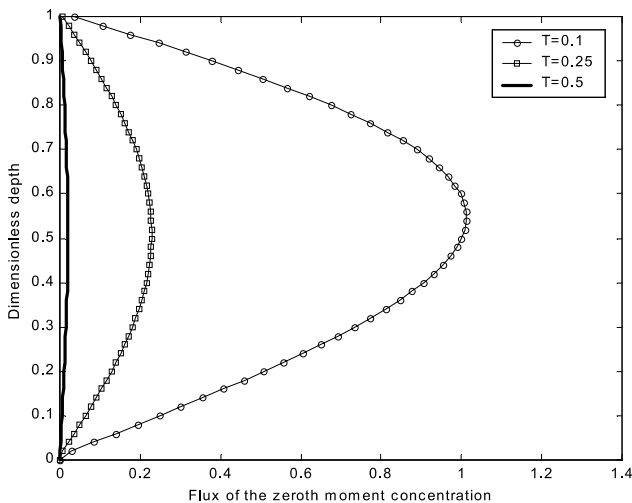


Fig. 7. Variation of the flux of the zeroth moment of concentration with depth for $D = 1$ at three different times.

found to greatly influence the transport characteristics in the river channel-bed interface. We also presented a comparison of the analytical model with experimental data measured in a laboratory setting [10,11]. The comparison was satisfactory despite the fact that the experimental measurements did not capture or did not intend to measure the macroscopic processes of the transport problem as well as the interaction among those processes. Future experimental studies need to measure the flow characteristics, such as the velocity profile, and the two-dimensional solute distribution in both the porous bed and the open channel. The model proposed in this paper is a useful tool to model and study water quality in rivers and sediment beds especially since the model parameters can be independently measured, and the sources of solute can be specified for either or both transport domains. In the absence of large-scale field studies, this model could be used not only to predict solute concentrations but also to estimate the impact of non-Gaussian solute distributions on the transfer of solutes across the interface through the inclusion of higher-order moments into the analysis. Further extensions of this model point to the need to include an advective term along the vertical dimension of the domain.

Acknowledgements

The first author acknowledges the support of the Boris A. Bakhmeteff Research Fellowship at Columbia University. The authors would like to thank M. Parlange, the editor, and the two anonymous reviewers of Advances in Water Resources for their detailed comments that greatly helped to improve the original manuscript.

Appendix A. Analytical derivations for the moments of concentration

A.1. Zeroth moment of concentration

The zeroth moment of concentration ($p = 0$) satisfies (23)–(29) and can be derived as the summation of a steady-state and transient solutions.

$$C_i(Y, T) = R_i^0(Y, T) + C_{i\infty}(Y), \tag{A.1}$$

where R_i^0 is the transient solution and $C_{i\infty}$ is the steady-state solution. Integrating twice, and using the boundary conditions, the steady-state solution is a constant:

$$C_{1\infty}^0 = C_{2\infty}^0 = \frac{\alpha m_1 + \beta m_2}{Y_1 + Y_2} = \alpha m_1 + \beta m_2. \tag{A.2}$$

Using separation of variables, we obtain

$$R_1^0 = \sum_{n=1}^{\infty} K_n \exp(-\lambda_n^2 T) [A_1 \cos(\lambda_n Y) + B_1 \sin(\lambda_n Y)], \tag{A.3}$$

$$R_2^0 = \sum_{n=1}^{\infty} K_n \exp(-\lambda_n^2 T) \cos\left(\frac{\lambda_n}{\sqrt{D}} Y\right), \tag{A.4}$$

where λ_n are the eigenvalues of the problem, and A_1, B_1 , and K_n are constants. Using the boundary conditions,

$$\begin{bmatrix} -\lambda \sin(\lambda) & \lambda \cos(\lambda) & 0 \\ \cos(\lambda Y_2) & \sin(\lambda Y_2) & -\cos\left(\frac{\lambda}{\sqrt{D}} Y_2\right) \\ -\lambda \sin(\lambda Y_2) & \lambda \cos(\lambda Y_2) & \lambda \sqrt{D} \sin\left(\frac{\lambda}{\sqrt{D}} Y_2\right) \end{bmatrix} \begin{bmatrix} A_1 \\ B_1 \\ 1 \end{bmatrix} = \begin{bmatrix} 0 \\ 0 \\ 0 \end{bmatrix}. \tag{A.5}$$

Solving the above system (Det = 0), the following equation is obtained:

$$\sqrt{D} \sin\left(\frac{\lambda}{\sqrt{D}} Y_2\right) \cos(\lambda Y_1) + \cos\left(\frac{\lambda}{\sqrt{D}} Y_2\right) \sin(\lambda Y_1) = 0. \tag{A.6}$$

We can solve for A_1 and B_1 :

$$A_1 = \cos\left(\frac{\lambda}{\sqrt{D}} Y_2\right) \cos(\lambda Y_2) + \sqrt{D} \sin\left(\frac{\lambda}{\sqrt{D}} Y_2\right) \sin(\lambda Y_2), \tag{A.7}$$

$$B_1 = \cos\left(\frac{\lambda}{\sqrt{D}} Y_2\right) \sin(\lambda Y_2) - \sqrt{D} \sin\left(\frac{\lambda}{\sqrt{D}} Y_2\right) \cos(\lambda Y_2), \tag{A.8}$$

where λ are the non-zero roots of Eq. (A.6). The coefficients K_n are determined using the initial conditions and the orthogonality of the sine and cosine functions. Since the values of λ are spaced at incommensurable intervals, the property of the sine and cosine being orthogonal cannot be established by simple integration. A proof is detailed in El-Habel [9].

$$K_n = \left\{ \frac{A_1 A_1}{\lambda_n} [\sin(\lambda_n) - \sin(\lambda_n Y_2)] - \frac{A_1 B_1}{\lambda_n} [\cos(\lambda_n) - \cos(\lambda_n Y_2)] + \frac{A_2 \sqrt{D}}{\lambda_n} \sin\left(\frac{\lambda_n Y_2}{\sqrt{D}}\right) \right\} / \left\{ A_1^2(H_1) + B_1^2(H_2) - \frac{A_1 B_1}{2\lambda_n} [\cos(2\lambda_n) - \cos(2\lambda_n Y_2)] + \frac{Y_2}{2} + \frac{\sqrt{D}}{4\lambda_n} \sin\left(\frac{2\lambda_n Y_2}{\sqrt{D}}\right) \right\}, \tag{A.9}$$

where

$$A_1 = \alpha m_1 \left(\frac{1}{Y_1} - 1 \right) - \beta m_2, \tag{A.10a}$$

$$A_2 = \beta m_2 \left(\frac{1}{Y_2} - 1 \right) - \alpha m_1, \tag{A.10b}$$

$$H_1 = \frac{Y_1}{2} + \frac{1}{4\lambda_n} [\sin(2\lambda_n) - \sin(2\lambda_n Y_2)], \tag{A.11a}$$

$$H_2 = \frac{Y_1}{2} - \frac{1}{4\lambda_n} [\sin(2\lambda_n) - \sin(2\lambda_n Y_2)]. \tag{A.11b}$$

A.2. First moment of concentration

An analysis of the variation in position of the solute cloud requires a solution for the first moment of the concentration, which is obtained using $p = 1$ in Eqs. (23)–(29). The solutions consist of a particular and a complementary solutions:

$$C_i^1 = f_{iH}^1(Y, T) + f_{iP}^1(Y, T) + g_i^1(Y), \tag{A.12}$$

where $f_{iH}^1(Y, T)$ is the complementary solution, $f_{iP}^1(Y, T)$ is the particular solution, and $g_i^1(Y)$ is the steady-state solution. The solutions for $g_i^1(\eta)$ satisfy two second-order ordinary differential equations. The solutions are

$$g_1^1 = (\alpha m_1 + \beta m_2) \left[W_{b0} \left(Y - \frac{Y^2}{2} \right) + W_{f0}^2 \left(\frac{Y}{2} - Y_2 Y + \frac{Y_2 Y^2}{2} - \frac{Y^3}{6} - \frac{Y}{6Y_1} - \frac{Y_2^2 Y}{2Y_1} + \frac{Y_2 Y}{2Y_1} + \frac{Y^4}{24Y_1} + \frac{Y_2^2 Y^2}{4Y_1} - \frac{Y^3 Y_2}{6Y_1} \right) - \text{Ve} \left(Y - \frac{Y^2}{2} \right) \right] + \frac{\alpha m_1 + \beta m_2}{D} \left\{ -\bar{W} \frac{Y_2^2}{2} + \text{Ve} \frac{Y_2^2}{2} + \frac{W_{b0} - \bar{W}}{\bar{K}} \left[Y_2 \exp(-\bar{K} Y_2) - \frac{1}{\bar{K}} \right] \right\}, \tag{A.13}$$

$$g_2^1 = \frac{\alpha m_1 + \beta m_2}{D} \left(-\bar{W} \frac{Y^2}{2} + \text{Ve} \frac{Y^2}{2} + \frac{W_{b0} - \bar{W}}{\bar{K}} \times \left\{ Y \exp(-\bar{K} Y_2) - \frac{1}{\bar{K}} - \exp[\bar{K}(Y - Y_2)] \right\} \right) + (\alpha m_1 + \beta m_2) \left[W_{b0} \left(Y_2 - \frac{Y_2^2}{2} \right) + W_{f0}^2 \left(\frac{Y_2}{2} - Y_2^2 + \frac{Y_2^3}{3} - \frac{Y_2}{6Y_1} + \frac{Y_2^2}{2Y_1} - \frac{Y_2^3}{2Y_1} + \frac{Y_2^4}{8Y_1} \right) - \text{Ve} \left(Y_2 - \frac{Y_2^2}{2} \right) \right]. \tag{A.14}$$

The above two equations present the asymptotic solution for the first moment of concentration. As for the particular solution, it can be written in the following form [26]:

$$f_{1P}^1 = \sum_{n=-1}^{\infty} K_n F_1(Y) \exp(-\lambda_n^2 T), \tag{A.15}$$

$$f_{2P}^1 = \sum_{n=-1}^{\infty} K_n F_2(Y) \exp(-\lambda_n^2 T). \tag{A.16}$$

F_1 and F_2 satisfy the following equations:

$$-\lambda^2 F_1 - \frac{d^2 F_1}{dY^2} = [W_1(Y) - \text{Ve}] [A_1 \cos(\lambda Y) + B_1 \sin(\lambda Y)], \tag{A.17}$$

$$-\lambda^2 F_2 - D \frac{d^2 F_2}{dY^2} = [W_2(Y) - \text{Ve}] \cos \left(\frac{\lambda}{\sqrt{D}} Y \right). \tag{A.18}$$

F_1 and F_2 are to be determined for each value of λ . Eqs. (A.17) and (A.18) are non-homogeneous linear differential equations of second order. The complete solution consists of a complementary and a particular solution. The particular solution is derived using the method of undetermined coefficients. The complete solution is

$$F_1 = M_1 \cos(\lambda Y) + N_1 \sin(\lambda Y) + (b_2 Y + c_2 Y^2 + d_2 Y^3) \times \sin(\lambda Y) + (b_1 Y + c_1 Y^2 + d_1 Y^3) \cos(\lambda Y), \tag{A.19}$$

$$F_2 = M_2 \cos \left(\frac{\lambda}{\sqrt{D}} Y \right) + N_2 \sin \left(\frac{\lambda}{\sqrt{D}} Y \right) + d_3 \exp(\bar{K} Y) \cos \left(\frac{\lambda}{\sqrt{D}} Y \right) + [b_4 Y + d_4 \exp(\bar{K} Y)] \sin \left(\frac{\lambda}{\sqrt{D}} Y \right), \tag{A.20}$$

where

$$b_1 = \frac{\Phi_1 B_1}{2\lambda} - \frac{\Phi_3 B_1}{4\lambda^3} - \frac{\Phi_2 A_1}{4\lambda^2}, \tag{A.21a, b, c}$$

$$c_1 = \frac{\Phi_2 B_1}{4\lambda} - \frac{\Phi_3 A_1}{4\lambda^2}, \quad d_1 = \frac{\Phi_3 B_1}{6\lambda},$$

$$b_2 = -\frac{\Phi_1 A_1}{2\lambda} + \frac{\Phi_3 A_1}{4\lambda^3} - \frac{\Phi_2 B_1}{4\lambda^2}, \tag{A.22a, b, c}$$

$$c_2 = \frac{\Phi_2 A_1}{4\lambda} - \frac{\Phi_3 B_1}{4\lambda^2}, \quad d_2 = -\frac{\Phi_3 A_1}{6\lambda},$$

$$d_3 = -\frac{\Phi_5}{D\bar{K}^2 + 4\lambda^2}, \quad b_4 = -\frac{\Phi_4}{2\lambda\sqrt{D}}, \tag{A.23a, b, c}$$

$$d_4 = -\frac{2\lambda\Phi_5}{(\sqrt{D}\bar{K}(D\bar{K}^2 + 4\lambda^2)},$$

and

$$\Phi_1 = W_{b0} - \text{Ve} - W_{f0}^2 Y_2 - \frac{W_{f0}^2 Y_2^2}{2Y_1}, \tag{A.24a, b}$$

$$\Phi_2 = W_{f0}^2 + \frac{W_{f0}^2 Y_2}{Y_1},$$

$$\Phi_3 = -\frac{W_{f0}^2}{2Y_1}; \quad \Phi_4 = \bar{W} - \text{Ve}, \tag{A.25a, b, c}$$

$$\Phi_5 = (W_{b0} - \bar{W}) \exp(-\bar{K} Y_2).$$

The constants in (A.19) and (A.20), namely M_1 , M_2 , N_1 , and N_2 are determined using the boundary conditions:

$$\begin{aligned} N_1 &= M_1 \tan(\lambda) + \Omega_1, \\ N_2 &= -d_4 - d_3 \bar{K} \frac{\sqrt{D}}{\lambda}, \end{aligned} \tag{A.26a, b}$$

$$M_2 = \frac{M_1 \Omega_2 + \Omega_3}{\cos\left(\frac{\lambda Y_2}{\sqrt{D}}\right)}, \quad M_1 = \frac{\Omega_4 + \Omega_5}{\Omega_6} \tag{A.27a, b}$$

in which

$$\Omega_1 = \frac{-b_1 - 2c_1 - 3d_1 - \lambda(b_2 + c_2 + d_2)}{\lambda} + \frac{\tan(\lambda)}{\lambda} \times [-b_2 - 2c_2 - 3d_2 + \lambda(b_1 + c_1 + d_1)], \tag{A.28a}$$

$$\Omega_2 = \cos(\lambda Y_2) + \sin(\lambda Y_2) \tan(\lambda), \tag{A.28b}$$

$$\begin{aligned} \Omega_3 &= \sin(\lambda Y_2) \Omega_1 + \cos(\lambda Y_2) (b_1 Y_2 + c_1 Y_2^2 + d_1 Y_2^3) \\ &+ \sin(\lambda Y_2) (b_2 Y_2 + c_2 Y_2^2 + d_2 Y_2^3) \\ &+ \cos\left(\frac{\lambda Y_2}{\sqrt{D}}\right) [-d_3 \exp(\bar{K} Y_2)] + \sin\left(\frac{\lambda Y_2}{\sqrt{D}}\right) \\ &\times \left[-d_4 \exp(\bar{K} Y_2) - b_4 Y_2 + d_4 + d_3 \bar{K} \frac{\sqrt{D}}{\lambda} \right], \end{aligned} \tag{A.28c}$$

$$\begin{aligned} \Omega_4 &= \cos(\lambda Y_2) (-b_1 - 2c_1 Y_2 - 3d_1 Y_2^2 - \lambda b_2 Y_2 \\ &- \lambda c_2 Y_2^2 - \lambda d_2 Y_2^3 - \lambda \Omega_1) \\ &+ \cos\left(\frac{\lambda Y_2}{\sqrt{D}}\right) [\lambda \sqrt{D} d_4 \exp(\bar{K} Y_2) \\ &+ \lambda \sqrt{D} b_4 Y_2 + D d_3 \bar{K} \exp(\bar{K} Y_2) + \lambda \sqrt{D} N_2], \end{aligned} \tag{A.28d}$$

$$\begin{aligned} \Omega_5 &= \sin(\lambda Y_2) (-b_2 - 2c_2 Y_2 - 3d_2 Y_2^2 + \lambda b_1 Y_2 \\ &+ \lambda c_1 Y_2^2 + \lambda d_1 Y_2^3) \\ &+ \sin\left(\frac{\lambda Y_2}{\sqrt{D}}\right) [-\lambda \sqrt{D} d_3 \exp(\bar{K} Y_2) + D b_4 \\ &+ D d_4 \bar{K} \exp(\bar{K} Y_2) - \lambda \sqrt{D} \tan\left(\frac{\lambda Y_2}{\sqrt{D}}\right) (\Omega_3)], \end{aligned} \tag{A.28e}$$

$$\begin{aligned} \Omega_6 &= -\lambda \sin(\lambda Y_2) + \lambda \cos(\lambda Y_2) \tan(\lambda) \\ &+ \lambda \sqrt{D} \tan\left(\frac{\lambda Y_2}{\sqrt{D}}\right) \Omega_2. \end{aligned} \tag{A.28f}$$

The complementary solution satisfies the following homogeneous problem:

$$\frac{\partial f_{1H}^1}{\partial T} - \frac{\partial^2 f_{1H}^1}{\partial Y^2} = 0, \tag{A.29}$$

$$\frac{\partial f_{2H}^1}{\partial T} - \gamma \frac{\partial^2 f_{2H}^1}{\partial Y^2} = 0. \tag{A.30}$$

The above two equations are identical to the equations describing the solution for C^0 . Using the method of separation of variables as described in the solution for the zeroth moment of concentration, one gets

$$f_{1,H}^1 = \sum_{n=1}^{\infty} K'_n \exp(-\alpha_n^2 T) [A'_1 \cos(\alpha_n Y) + B'_1 \sin(\alpha_n Y)] \tag{A.31}$$

$$f_{2,H}^1 = \sum_{n=1}^{\infty} K'_n \exp(-\alpha_n^2 T) \cos\left(\frac{\alpha_n}{\sqrt{D}} Y\right) \tag{A.32}$$

Similar to λ , α satisfies (A.6). Also, solving for A'_1 , B'_1 , and K'_n we get

$$\begin{aligned} A'_1 &= \cos\left(\frac{\alpha}{\sqrt{D}} Y_2\right) \cos(\alpha Y_2) \\ &+ \sqrt{D} \sin\left(\frac{\alpha}{\sqrt{D}} Y_2\right) \sin(\alpha Y_2), \end{aligned} \tag{A.33}$$

$$\begin{aligned} B'_1 &= \cos\left(\frac{\alpha}{\sqrt{D}} Y_2\right) \sin(\alpha Y_2) \\ &- \sqrt{D} \sin\left(\frac{\alpha}{\sqrt{D}} Y_2\right) \cos(\alpha Y_2), \end{aligned} \tag{A.34}$$

$$\begin{aligned} K'_n &= \left\{ \int_{Y_2}^1 (g_1^1 - f_{1P}^1)_{T=0} [A'_1 \cos(\alpha_n Y) \right. \\ &+ B'_1 \sin(\alpha_n Y)] dY + \int_0^{Y_2} (g_2^1 - f_{2P}^1)_{T=0} \\ &\times \cos\left(\frac{\alpha_n}{\sqrt{D}} Y\right) dY \left. \right\} / \left\{ \int_{Y_2}^1 [A'_1 \cos(\alpha_n Y) \right. \\ &+ B'_1 \sin(\alpha_n Y)]^2 dY + \int_0^{Y_2} \cos^2\left(\frac{\alpha_n}{\sqrt{D} Y}\right) dY \left. \right\}. \end{aligned} \tag{A.35}$$

A.3. Second moment of concentration

A more detailed description of the contaminant description needs an expression for C^2 ($p = 2$). The main problem facing the derivation of a complete solution for the above two equations is the fact that the expressions for C^1 are complicated. However, a solution that contains the terms that do not vanish as $T \rightarrow \infty$ can be derived, an approach previously followed by Aris [2]. Dropping the time derivative term the following equations are obtained:

$$\frac{d^2 C_1^2}{dY^2} = -2(\alpha m_1 + \beta m_2) - 2[W_1(Y) - \text{Ve}] g_1^1, \tag{A.36}$$

$$\frac{d^2 C_2^2}{dY^2} = -2(\alpha m_1 + \beta m_2) - \frac{2}{D} [W_2(Y) - \text{Ve}] g_2^1. \tag{A.37}$$

The solutions of the above two equations are obtained simply by integrating twice using the proper boundary conditions. However, the derivation is quite cumbersome and will not be presented here for brevity reasons. The solutions are

$$C_1^2 = (\alpha m_1 + \beta m_2) [\Gamma_1(Y) + \Gamma_2(Y_2)], \tag{A.38}$$

$$C_2^2 = (\alpha m_1 + \beta m_2) [\Gamma_2(Y) + \Gamma_1(Y_2)], \tag{A.39}$$

where

$$\begin{aligned} \Gamma_1(Y) = & \frac{Y^2}{2}(-2 - 2\Phi_1 p_1) + \frac{Y^3}{3}(-\Phi_1 p_2 - \Phi_2 p_1) \\ & + \frac{Y^4}{4} \left(-2 \frac{\Phi_1 p_3}{3} - 2 \frac{\Phi_2 p_2}{3} - 2 \frac{\Phi_3 p_1}{3} \right) \\ & + \frac{Y^5}{5} \left(-2 \frac{\Phi_1 p_4}{4} - 2 \frac{\Phi_2 p_3}{4} - 2 \frac{\Phi_3 p_2}{4} \right) \\ & + \frac{Y^6}{6} \left(-2 \frac{\Phi_1 p_5}{5} - 2 \frac{\Phi_2 p_4}{5} - 2 \frac{\Phi_3 p_3}{5} \right) \\ & + \frac{Y^7}{7} \left(-2 \frac{\Phi_2 p_5}{6} - 2 \frac{\Phi_3 p_4}{6} \right) + \frac{Y^8}{8} \left(-2 \frac{\Phi_3 p_5}{7} \right) \\ & + 2Y + Y\Phi_1 \left(2p_1 + \frac{2p_2}{2} + \frac{2p_3}{3} + \frac{2p_4}{4} + \frac{2p_5}{5} \right) \\ & + Y\Phi_2 \left(\frac{2p_2}{3} + \frac{2p_3}{4} + \frac{2p_4}{5} + \frac{2p_5}{6} \right) \\ & + Y\Phi_3 \left(\frac{2p_1}{3} + \frac{2p_2}{4} + \frac{2p_3}{5} + \frac{2p_4}{6} + \frac{2p_5}{7} \right), \end{aligned} \quad (A.40)$$

$$\begin{aligned} \Gamma_2(Y) = & Y^2 \left(-1 - \frac{\Phi_4 q_1}{D} \right) + Y^3 \left(-\frac{\Phi_4 q_2}{3D} \right) \\ & + Y^4 \left(-\frac{\Phi_4 q_3}{6D} \right) + \exp[\bar{K}(2Y - Y_2)] \\ & \times \left(-2 \frac{\Phi_5 q_4}{4D\bar{K}^2} \right) + \exp(\bar{K}Y) \left[-2 \frac{\Phi_4 q_4}{D\bar{K}^2} \right. \\ & \times \exp(-\bar{K}Y_2) - 2 \frac{\Phi_5 q_1}{D\bar{K}^2} - 2 \frac{\Phi_5 q_3}{D\bar{K}^2} Y^2 \\ & \left. - 2 \frac{\Phi_5 q_2}{D\bar{K}^3} (\bar{K}Y - 2) + 4 \frac{\Phi_5 q_3}{D\bar{K}^4} (2\bar{K}Y - 3) \right] \\ & + Y \exp(\bar{K}Y_2) \left(-\frac{\Phi_5 q_4}{D\bar{K}} - 2 \frac{\Phi_4 q_4}{D\bar{K}} \right) \\ & - 2Y \frac{\Phi_5}{D\bar{K}} \left(q_1 - \frac{q_2}{\bar{K}} + \frac{2q_3}{\bar{K}^2} \right), \end{aligned} \quad (A.41)$$

and

$$\begin{aligned} p_1 = & \frac{1}{D} \left\{ -\bar{W} \frac{Y_2^2}{2} + \text{Ve} \frac{Y_2^2}{2} + \frac{W_{b0} - \bar{W}}{\bar{K}} \right. \\ & \left. \times \left[Y_2 \exp(-\bar{K}Y_2) - \frac{1}{\bar{K}} \right] \right\}, \end{aligned} \quad (A.42a)$$

$$p_2 = W_{b0} + W_{f0}^2 \left(\frac{1}{2} - Y_2 - \frac{1}{6Y_1} - \frac{Y_2^2}{2Y_1} - \frac{Y_2}{2Y_1} \right) - \text{Ve}, \quad (A.42b)$$

$$p_3 = -\frac{W_{b0}}{2} + W_{f0}^2 \left(\frac{Y_2}{2} + \frac{Y_2^2}{4Y_1} \right) + \frac{\text{Ve}}{2}, \quad (A.42c)$$

$$p_4 = W_{f0}^2 \left(-\frac{1}{6} - \frac{Y_2}{6Y_1} \right), \quad (A.42d)$$

$$p_5 = \frac{W_{f0}^2}{24Y_1}, \quad (A.42e)$$

$$\begin{aligned} q_1 = & W_{b0} \left(Y_2 - \frac{Y_2^2}{2} \right) + W_{f0}^2 \left(\frac{Y_2}{2} - Y_2^2 + \frac{Y_2^3}{3} - \frac{Y_2}{6Y_1} + \frac{Y_2^2}{2Y_1} \right. \\ & \left. - \frac{Y_2^3}{2Y_1} + \frac{Y_2^4}{8Y_1} \right) - \text{Ve} \left(Y_2 - \frac{Y_2^2}{2} \right), \end{aligned} \quad (A.43a)$$

$$q_2 = \frac{1}{D} \left\{ \frac{W_{b0} - \bar{W}}{\bar{K}} [\exp(-\bar{K}Y_2)] \right\}, \quad (A.43b)$$

$$q_3 = \frac{1}{D} \left(-\frac{\bar{W}}{2} + \frac{\text{Ve}}{2} \right), \quad (A.43c)$$

$$q_4 = \frac{1}{D} \left(-\frac{W_{b0} - \bar{W}}{\bar{K}^2} \right). \quad (A.43d)$$

References

- [1] Abramowitz M, Stegun IA. Handbook of mathematical functions. New York: Dover; 1972.
- [2] Aris R. On the dispersion of a solute in a fluid flowing through a tube. Proc R Soc London, Ser A 1956;235:67–77.
- [3] Aris R. The longitudinal diffusion coefficient in flow through a tube with stagnant pockets. Chem Eng Sci 1959;11:194–8.
- [4] Basha HA. Analytical model of two-dimensional dispersion in laterally nonuniform axial velocity distributions. J Hydraul Eng 1997;123(10):853–62.
- [5] Bencala KE. Interactions of solutes and streambed sediment: 2. A dynamic analysis of coupled hydrologic and chemical processes that determine solute transport. Water Resour Res 1984; 20(12): 1804–14.
- [6] Beavers GS, Joseph DD. Boundary conditions at a naturally permeable wall. J Fluid Mech 1967;30:197–207.
- [7] Chatwin PC. The approach to normality of the concentration distribution of solute in a solvent flowing along a straight pipe. J Fluid Mech 1970;51:321–52.
- [8] Chatwin PC. A calculation illustrating effects of the viscous sub-layer on longitudinal dispersion. Q J Mech Appl Math 1973;26: 427–39.
- [9] El-Habel F. Solute transport in open channel flows and porous beds. PhD Dissertation, Columbia University, 1998.
- [10] Elliott AH, Brooks NH. Transfer of nonsorbing solutes to a streambed with bed forms: theory. Water Resour Res 1997a;33:123–36.
- [11] Elliott AH, Brooks NH. Transfer of nonsorbing solutes to a streambed with bed forms: laboratory experiments. Water Resour Res 1997b;33:137–51.
- [12] Engelund F. A practical approach to self-preserving turbulent flows. Acta Polytech Scand 1964.
- [13] Engelund F. Instability of erodible beds. J Fluid Mech 1970; 42:225–44.
- [14] Fischer HB, List EJ, Koh RY, Imberger J, Brooks NH. Mixing in inland and coastal waters. New York: Academic Press; 1979.
- [15] Fischer HB. The mechanics of dispersion in natural streams. J Hydraul Div Proc ASCE 1967;93:187–216.
- [16] Guven O, Molz FJ, Melville JG. An analysis of dispersion in a stratified aquifer. Water Resour Res 1984;20:1337–54.
- [17] Hinze JO. Turbulence: an introduction to its mechanics and theory. 2nd ed. New York: McGraw-Hill; 1975.
- [18] Nagaoka H, Ohgaki S. Mass transfer mechanism in a porous riverbed. Water Res 1990;24(4):417–25.
- [19] Nordin CF, Sabol GV. Estimating average sediment yield from annual streamflow and sediment records. Proceedings of the IAHR International Symposium on River Mechanics, Bangkok 1973:93–104.

- [20] Nordin CF, Troutman BM. Longitudinal dispersion in rivers: the persistence of skewness in observed data. *Water Resour Res* 1980;16:123–8.
- [21] Ochoa-Tapia JA, Whitaker S. Momentum transfer at the boundary between a porous medium and a homogeneous fluid – I. Theoretical development. *Int J Heat Mass Transfer* 1995;38(14):2635–46.
- [22] Purnama A. The effect of dead zones on longitudinal dispersion in streams. *J Fluid Mech* 1988;186:351–77.
- [23] Rudraiah N. Coupled parallel flows in a channel and a bounding porous medium of finite thickness. *J Fluids Eng* 1985;107:322–9.
- [24] Rutherford JC, Latimer GJ, Smith RK. Bedform mobility and benthic oxygen uptake. *Water Resour Res* 1988;27:1454–558.
- [25] Sayre WW. *Hydraulics Papers*, No. 3. Colorado State University, Fort Collins, 1968.
- [26] Sumer BM. Mean velocity and longitudinal dispersion of heavy particles in turbulent open-channel flow. *J Fluid Mech* 1974;65:11–28.
- [27] US Environmental Protection Agency, Report Brochure: National Water Quality Inventory: 1996 Report to Congress, Background Section [online]. Office of Water, Washington DC, 1998. Available: <http://www.epa.gov/OW/resources/brochure/broch2.html> (28 March 2000).
- [28] Valentine EM, Wood IR. Longitudinal dispersion with dead zones. *J Hydraul Div ASCE* 1977;103:975–90.
- [29] Zhou D, Mendoza CC. Flow through porous bed of turbulent stream. *J Eng Mech, ASCE* 1993;119:365–83.